Front. Optoelectron. 2012, 5(4): 390–394
DOI 10.1007/s12200-012-0287-5

RESERACH ARTICLE

Influence of facet reflection of SOA on SOA-integrated SGDBR laser

Tan SHU[1], Yonglin YU (✉)[1], Hui LV[1], Dexiu Huang[1], Kai SHI[2], Liam BARRY[2]

1 Wuhan National Laboratory for Optoelectronics, College of Optoelectronic Science and Engineering, Huazhong University of Science & Technology, Wuhan 430074, China
2 The Rince Institute, Dublin City University, Glasnevin, Dublin 9, Ireland

Abstract A combined model of the transmission-line laser model (TLLM) and the digital filter approach is developed to simulate the shuttering characteristic of a semiconductor optical amplifier (SOA), which is integrated with a sampled grating distributed Bragg reflector (SGDBR) laser, to create a so called SOA-SGDBR laser. The SOA section acts as a shutter to blank the laser output during wavelength switching events. Simulated results show that the turn-on edge of the SOA blanking process will oscillate when the facet reflection of SOA is relatively high. This phenomenon is also observed by experiments.

Keywords sampled grating distributed Bragg reflector (SGDBR) laser, semiconductor optical amplifier (SOA), transmission-line laser model (TLLM), digital filter approach

1 Introduction

Widely tunable sampled grating distributed Bragg reflector (SGDBR) lasers have attracted much attention in high-capacity photonic networks based on dense wavelength division multiplexing and wavelength routing [1]. SGDBR lasers provide wide tuning range, fast wavelength switching time, and excellent side-mode suppression ratio (SMSR). Furthermore, SGDBR lasers have an important advantage of being easily monolithically integrated with other devices such as semiconductor optical amplifier (SOA) and electro-absorption modulator (EAM) to create photonic integrated circuits with more functionality without significantly increasing the fabrication complexity [2]. The work presented here is concentrated on an SOA-integrated SGDBR laser. The integrated SOA in front of the SGDBR laser, can be used not only as a variable optical power controller, but also as a shutter during fast wavelength switching of the laser. It has been demonstrated that an integrated SOA can be used to blank the spurious modes generated by the tunable DBR lasers during wavelength channel switches [3,4]. Previous results also indicated that high facet reflection of an integrated SOA section will degrade the SMSR and linewidth of such lasers [5].

In this paper, the influence of facet reflection of the integrated SOA on blanking characteristics of the SOA-SGDBR devices is investigated by simulations and experiments.

Received September 3, 2012; accepted September 14, 2012

E-mail: yonglinyu@mail.hust.edu.cn

2 Model description

A combined model of the transmission-line laser model (TLLM) with the digital filter approach is developed to simulate the blanking characteristic of an SOA integrated with an SGBDR laser. The scheme of the combined model is illustrated in Fig. 1. The active regions, the phase regions and the SOA regions can be described easily in the time domain by the TLLM [6]. For the two grating reflectors of the SGDBR lasers, however, it is difficult to represent them in the time domain, due to their complex structure of sampled grating. Here, the transfer matrix method (TMM, a frequency domain model) is used to characterize the front and rear sampled grating (F/RSG) regions, and then the reflection and transmission coefficients of F/RSG are coupled into the proposed TLLM via the digital filter approach. It has been verified that signals in time domain and frequency domain can be transformed into each other by using the finite impulse response (FIR) filter as a bridge [7,8].

The basic principle of the TLLM is that the laser cavity length L can be longitudinally divided into a number of equal length sections s, with a length ΔL. In each section, a

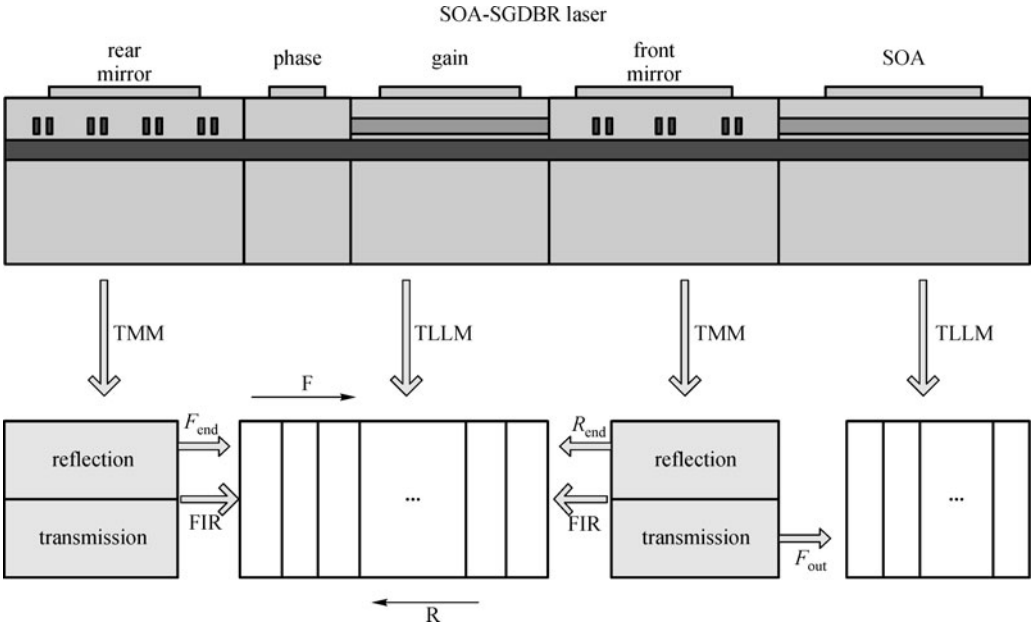

Fig. 1 Schematic of SOA-integrated SGDBR model. The active, phase and SOA sections are modeled using TLLM, while the F/RSG sections are first simulated by TMM, and then transformed into time domain via FIR

scattering matrix $\boldsymbol{S}$ is used to represents the optical process, including stimulation emission, spontaneous emission, and attenuation. The matrices of these sections are then connected by transmissionlines, which account for propagation delays of the optical wave. Each section includes a propagation delay of ΔT, which is related to the laser's cavity length and the group velocity v_g inside the cavity, and is given by

$$\Delta L = v_g \Delta T. \tag{1}$$

The connecting processes can be represented by a connecting matrix $\boldsymbol{C}$. From the iterations of scattering and connecting processes, the output optical field in the time domain can be obtained. Then, with the help of the fast Fourier transform (FFT), the laser output spectrum can be easily acquired. The independent carrier rate equation is used in each section to govern the carrier-photon interaction.

The scattering processes represent the optical process, including stimulated emission, spontaneous emission, and attenuation, in each section, and can be expressed as [9]

$$_kA(n)^{\mathrm{r}} = S \cdot {}_kA(n)^{\mathrm{i}} + {}_kA(n)^{\mathrm{s}}, \tag{2}$$

where $_kA(n)^{\mathrm{i}}$ is the incident wave at the input of the n section at the k time step, $_kA(n)^{\mathrm{r}}$ is the reflected wave from that section, and $_kA(n)^{\mathrm{s}}$ is the wave due to the spontaneous emission. $\boldsymbol{S}$ represents the scattering matrix.

The connection matrix describes the cross coupling between forward and backward traveling waves. It provides the incident wave of the scattering section from the reflected wave of the previous section, which may be described by

$$_{k+1}A(n)^{\mathrm{i}} = \boldsymbol{C} \cdot {}_kA(n)^{\mathrm{r}}. \tag{3}$$

F/RSG sections are first modeled by TMM [10,11] to get the reflection and transmission coefficients, then the FIR filter coefficients in the time domain $x(t)$ can be obtained easily by a reverse FFT transformation of the reflection and transmission coefficient function in the frequency domain, is given by [7]

$$x(t) = \frac{1}{M}\sum_{k=0}^{M-1} X(f)\mathrm{e}^{2\pi \mathrm{j}kf\Delta t}, \tag{4}$$

where $X(f)$ represents the reflection or transmission coefficients of FSR/RSG sections in the frequency domain.

The transmitted output optical field or the reflected field can be expressed by the M input field y^k and reflectivity and transmission FIR filter coefficients at the specific time k as [7]

$$F_{\mathrm{out}}^n = \sum_{k=0}^{M} x^k(t) y^{n-k}, \tag{5}$$

where $x^k(t)$ are the digital filter coefficients.

3 Simulation and experiment results

The SOA integrated SGDBR laser for simulation includes a 450-μm-long active section, a 150-μm-long phase

section, a 600-μm-long SOA section, a 10-period front sampled-grating mirror with 6-μm-wide bursts using a 58.5-μm period and a 12-period rear sampled-grating mirror with 6-μm-wide bursts and 64.5-μm period. Other simulation parameters used are given in Table 1.

Table 1 Simulation parameters

parameter		value
waveguide width		2 μm
waveguide thickness		0.05 μm
waveguide loss	active region	3000 m^{-1}
	pssive region	200 m^{-1}
waveguide confinement factor	active region	0.35
	passive region	0.5
effective refractive index		3.23
nonradioactive linear recombination coefficient		$1 \times 10^{8}\ s^{-1}$
bimolecular recombination coefficient		$1 \times 10^{-16}\ m^{3} \cdot s^{-1}$
auger recombination coefficient	active region	$2.5 \times 10^{-41}\ m^{6} \cdot s^{-1}$
	passive region	$7 \times 10^{-41}\ m^{6} \cdot s^{-1}$

The active, FSG, RSG and phase currents of the SGDBR laser are kept at 100, 3, 8, and 0 mA, respectively, to ensure that the laser has a stable output power to be launched into the SOA section. Simulated SOA gain versus the bias current of the SOA section is shown in Fig. 2. As can be seen from Fig. 2, the bias current of the SOA section needs to be switched from over 100 to 0 mA in order to get enough output power suppression for blanking applications.

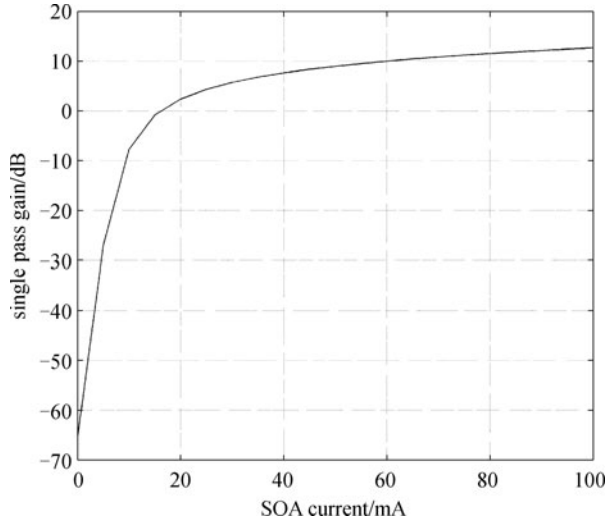

Fig. 2 SOA gain versus with bias current of SOA section

Blanking characteristics of the SOA-SGDBR laser are simulated. The bias current of the integrated SOA section is first switched between 120 and 0 mA, under two cases of facet reflections of the SOA. Figure 3(a) is the case which the facet reflection of the SOA is 10^{-4}, while Fig. 3(b) is the case which the facet reflection of the SOA is 10^{-3}. We can see that there is a small oscillation on the turn-on edge when the facet reflection increases to 10^{-3}. The oscillation can be observed more clearly when the bias current of the SOA increases. Figure 4 shows the simulated results when the bias current of the SOA is switched between 160 and 0 mA, under same two cases of facet reflections of the SOA. In comparison with Fig. 3(b), the oscillation on the turn-on edge in Fig. 4(b) is much more pronounced.

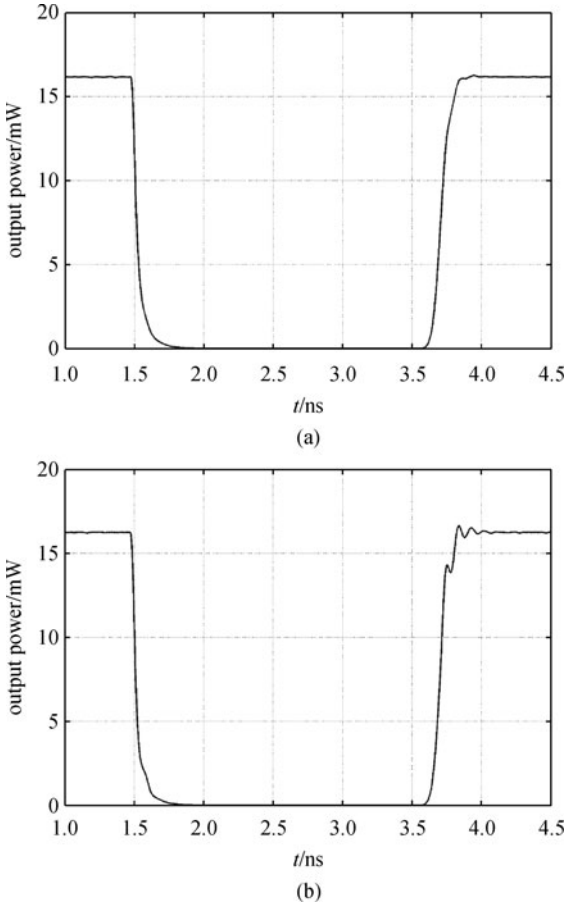

Fig. 3 SOA shuttering curve from 120 to 0 mA when facet reflection is (a) 10^{-4} and (b) 10^{-3}

From Figs. 3 and 4, we can find that the turn-on edge of the blanking process will oscillate when the facet reflection of the SOA is increased. Meanwhile, higher bias current into the SOA section will aggravates this oscillation.

We attribute the oscillation phenomenon to unstable optical output from the SGDBR laser. With the help of the developed model, we could investigate more detail of this phenomenon. The active, FSG, RSG and phase current of SGDBR laser are set as the above currents to ensure that

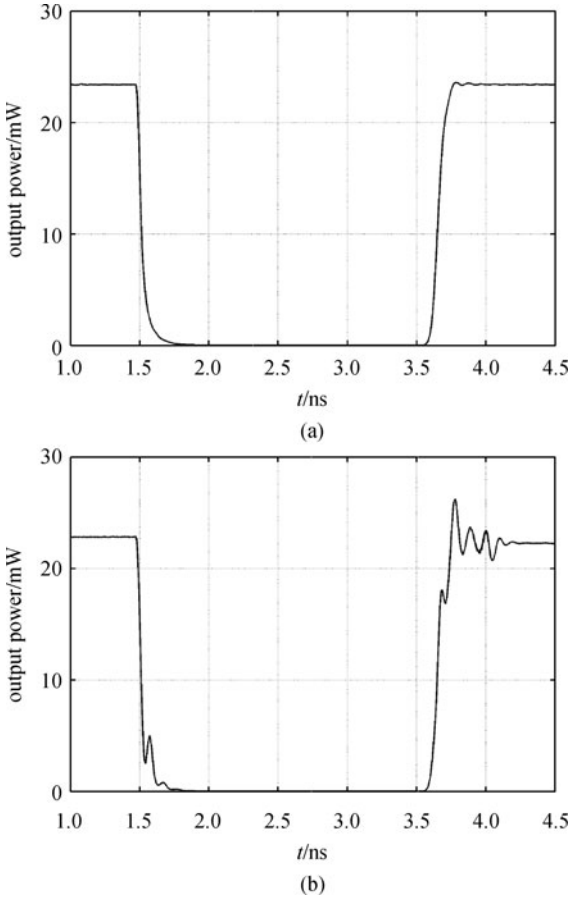

Fig. 4 SOA switching curve from 160 to 0 mA when facet reflection is (a) 10^{-4} and (b) 10^{-3}

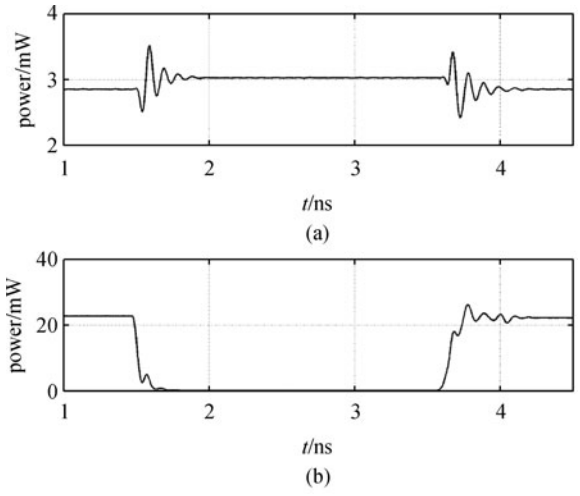

Fig. 5 Output power at facet of FSG (a) and SOA (b) when facet reflection is 10^{-3}

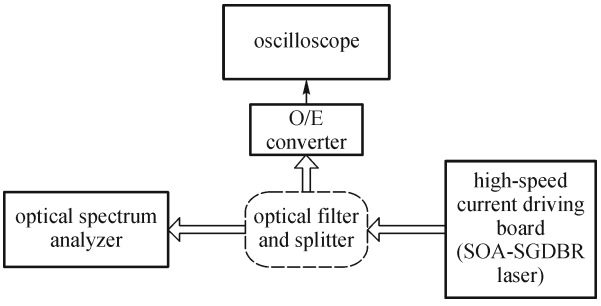

Fig. 6 Experimental set-up of wavelength switching and SOA blanking

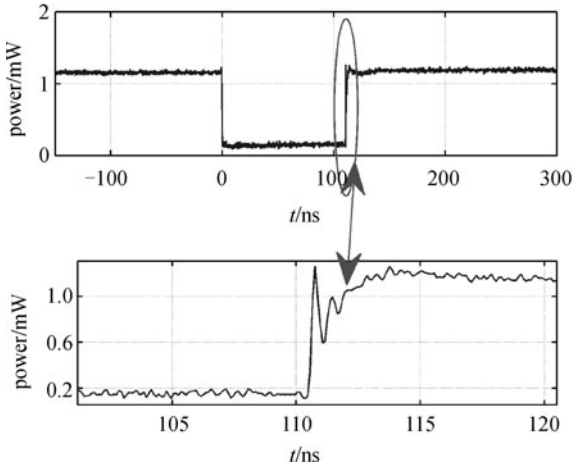

Fig. 7 Measured result of evolution of SOA blanking, bias current of SOA section is switched between 140 and 0 mA

the SGDBR laser has a stable output field to be launched into the SOA section. The output powers at the facet of the FSG section and the SOA section are simulated respectively, as shown in Fig. 5, where the facet reflection of the SOA is 10^{-3}. Due to the high facet reflection of the SOA, the reflected optical field from the SOA section results in an unstable output field from the SGDBR laser, which then affects the final output of the SOA section in turn, as shown in Fig. 5.

The oscillation on the turn-on edge during the SOA shuttering can be observed by experiments as well. Figure 6 shows the experimental set-up. To achieve fast control of the SOA-integrated SGDBR device, a high-speed current driving board has been developed which has a similar design with the one in Ref. [12]. In this case, an additional current driving circuit for the SOA section was included. The output of the SOA-integrated SGDBR lasers is directed to an optical spectrum analyzer (OSA) and an oscilloscope. Figure 7 reveals measured results of evolution of the output from the SOA under the blanking, where bias current of SOA section is switched between 140 and 0 mA.

4 Conclusions

We investigated the influence of facet reflection of the integrated SOA on blanking characteristics of the SOA-SGDBR laser by both simulations and experiments. Oscillation occurs on the turn-on edge of the SOA blanking process when the facet reflection is relatively high, and it can be aggravated by larger bias current into the SOA section. This is due to the facet reflection of the SOA, which causes the power fluctuation of the output of the SGDBR laser.

Acknowledgements This work was supported in part by the International S&T Cooperation Program of China (No. 1016), the National Natural Science Foundation of China (Grant No. 60677024), and the Specialized Research Fund for the Doctoral Program of Higher Education (SRFDP) (No. 20100142110045).

References

1. Buus J, Murphy E J. Tunable lasers in optical networks. IEEE Journal of Lightwave Technology, 2006, 24(1): 5–11
2. Coldren L A, Fish G, Akulova Y, Barton J S, Johansson L, Coldren C W. Tunable semiconductor lasers: a tutorial. IEEE Journal of Lightwave Technology, 2004, 22(1): 193–202
3. Ponnampalam L, Barlow R, Whitbread N D, Robbins D J, Busico G, Duck J P, Ward A J. Reid D C J, Williams P J. Dynamic control of wavelength switching and shuttering operations in a broadband tunable DS-DBR laser module. In: Proceedings of Optical Fiber Communication Conference Technical Digest, 2005, OTuE3
4. Lv H, Shu T, Yu Y L, Huang D X, Dong L, Zhang R K. Fast power control and wavelength switching in a tunable SOA-integrated SGDBR laser. In: Proceedings of the 14th OptoElectronics and Communications Conference, 2009, ThPD4
5. Ward A J, Robbins D J, Busico G, Barton E, Ponnampalam L, Duck J P, Whitbread N D, Williams P J, Reid D C J, Carter A C, Wale M J. Widely tunable DS-DBR laser with monolithically integrated SOA: design and performance. IEEE Journal on Selected Topics in Quantum Electronics, 2005, 11(1): 149–156
6. Lowery A J. Transmission-line modeling of semiconductor lasers: the transmission-line laser model. International Journal of Numerical Modeling: Electronic Networks, Devices and Fields, 1989, 2: 249–265
7. Li W, Huang W P, Li X. Digital filter approach for simulation of a complex integrated laser diode based on the traveling-wave model. IEEE Journal of Quantum Electronics, 2004, 40(5): 473–480
8. Dong L, Zhang R K, Wang D L, Zhao S Z, Jiang S, Yu Y L, Liu S H. Modeling widely tunable sampled-grating DBR lasers using traveling-wave model with digital filter approach. IEEE Journal of Lightwave Technology, 2009, 27(15): 3181–3188
9. Lowery A J. New dynamic model for multimode chirp in DFB semiconductor lasers. IEE Proceeings, 1990, 137(10): 293–300
10. Shi K, Yu Y L, Zhang R K, Liu W, Barry L P. Static and dynamic analysis of side-mode suppression of widely tunable sampled grating DBR (SG-DBR) lasers. Optics Communications, 2009, 282 (1): 81–87
11. Björk G, Nilsson O. A new exact and efficient numerical matrix theory of complicated laser structures: properties of asymmetric phase-shifted DFB lasers. IEEE Journal of Lightwave Technology, 1987, 5(1): 140–146
12. Lv H, Yu Y L, Huang D X, Shu T. A fast optical wavelength-tunable transmitter with a linear thermoelectric cooler driver. IEEE Electron Device Letters, 2009, 30(4): 353–355